Characterization of RNA interference in the model cnidarian *Nematostella vectensis* reveals partial target silencing but lack of small RNA amplification

Yael Admoni[1], Magda Lewandowska[1], Reuven Aharoni[1], Junchao Shi[2,3], Xudong Zhang[2], Qi Chen[2], Yehu Moran[1]

[1]Department of Ecology, Evolution and Behavior, Alexander Silberman Institute of Life Sciences, Faculty of Science, Hebrew University of Jerusalem, Jerusalem 9190401, Israel

[2]Molecular Medicine Program, Department of Human Genetics, and Division of Urology, Department of Surgery, School of Medicine, University of Utah, Salt Lake City, Utah, USA

[3] Present address: China National Centre for Bioinformation and Beijing Institute of Genomics, Chinese Academy of Sciences, Beijing 100101, China

Corresponding authors: Yael Admoni (yael.admoni@mail.huji.ac.il); Yehu Moran (yehu.moran@mail.huji.ac.il)

Short title: RNA interference in a cnidarian model

Abstract

RNA interference (RNAi) is an antiviral mechanism based on processing of viral double-stranded RNA (dsRNA) into short interfering RNAs (siRNAs) leading to dsRNA destruction. It is considered as an ancestral mechanism which invertebrates rely on for defense against viruses, while vertebrates have evolved instead the interferon pathway. Recent studies showed that sea anemones, members of the basally-branching phylum Cnidaria, might possess an antiviral response with more vertebrate characteristics than previously thought; however, it is unknown whether cnidarians also employ RNAi as an immune response similarly to nematodes and insects. In this study we characterize the antiviral RNAi response in the model cnidarian *Nematostella vectensis*. We injected dsRNA with GFP sequence to GFP-expressing transgenic zygotes and show that siRNAs mapping to the GFP sequence are generated and induce a moderate but significant knockdown of GFP expression. In addition, we find no evidence of secondary siRNA generation, despite their crucial role in the amplification of antiviral response in other organisms. Notably, RNAi pathway components are specifically upregulated upon dsRNA injection while microRNA pathway components are downregulated. Overall, our findings reveal that *N. vectensis* possesses an antiviral RNAi system with no secondary amplification, suggesting that it serves only as a short-term antiviral mechanism.

Introduction

RNA interference (RNAi) is a gene expression regulation mechanism based on short 20-30 nucleotide long RNA molecules that lead to silencing of a specific target. The two major RNAi pathways are the microRNA (miRNA) pathway that targets mostly endogenous protein coding genes and the short interfering RNA (siRNA) pathway that provides defense against transposons and viral infection (1,2). The siRNA pathway is assumed to be the main antiviral immune response mechanism of invertebrates, based on its ancestral origin and studies of common invertebrate models such as the nematode *Caenorhabditis elegans* and the fly *Drosophila melanogaster* (3–5). In vertebrates, the RNAi system was shown to remain only in specific tissues or developmental stages, and in general their main antiviral innate immune

response is instead the interferon pathway (6–9). The RNAi mechanism is based on detection of double-stranded RNA (dsRNA) by cellular receptors that leads to processing of the dsRNA by RNase III Dicer into 20-25 bases long primary siRNAs (10–12). These siRNAs are loaded into Argonaute (AGO) proteins that carry them to the target viral RNA and apply mechanisms to prevent its expression (13). As an important step, the primary response is amplified by the production of secondary siRNAs that greatly increase target silencing and prolong the response. In nematodes and plants, RNA-dependent RNA polymerases (RdRPs) are responsible for secondary siRNA production (14–16), whereas in flies the amplification is RdRP-independent and is mediated by reverse transcriptases (17). In *C. elegans*, secondary siRNAs are typified by carrying 5' triphosphate modification and they are 22 nucleotide long and tend to exhibit sequence biases (18–21). *D. melanogaster* also generates secondary antiviral siRNAs with 5' triphosphate modification, which are made by an as-yet unidentified reverse transcriptase (17,22). Antiviral RNAi has been well described in nematodes, insects, and plants; however, major gaps remain in its evolutionary history as it has not been characterized in many lineages including early branching metazoans, especially as both insects and nematodes belong to the Ecdysozoa.

In this study, we investigate the antiviral immune response in the sea anemone *Nematostella vectensis*, a model organism representing the phylum Cnidaria that diverged from most other animals over 600 million years ago (23,24). Cnidaria is comprised of Anthozoa (sea anemones and corals) and Medusozoa (jellyfish and hydras) and its phylogenetic position provides unique opportunities to explore evolutionary processes (25). Interestingly, despite their basal position some cnidarians show unexpected complexity in their antiviral pathways (26,27), and so far, there have been contradicting evidence regarding the functionality of the antiviral RNAi pathway in cnidarians.

First, *N. vectensis* possesses homologs to RNAi-related components such as AGO2, Dicer1 and three RdRPs that were shown to be upregulated upon injection of the viral dsRNA mimic, polyinosinic:polycytidylic acid (poly(I:C)) (26). This could point to activation of the antiviral

siRNA system; however, *N. vectensis* also has homologs to components of the interferon pathway, such as Interferon Regulatory Factors (26–28). In *N. vectensis*, interferon-related components are upregulated following poly(I:C) injection along with RNAi-related genes and it is unclear if one of these pathways plays a more major role in the antiviral response (26).

Second, all cnidarians employ a miRNA system, hence possess homologs to components of the RNAi system such as AGO and Dicer. In *N. vectensis*, AGO paralogs are specialized in carrying distinct populations of small RNAs, with AGO1 carrying only miRNAs and AGO2 carrying both miRNAs and endogenous siRNAs (29). In the medusozoan *Hydra magnipapillata* RNAi was shown to be functioning and dsRNA is used as driver of gene knockdown by electroporation or feeding (30,31). In the sea anemone *Exaiptasia diaphana* (previously called *Aiptasia pallida*) dsRNA was shown to be effective when delivered by soaking (32); however, no further studies reported the successful employment of this method in *Exaiptasia* or other sea anemones in the last 17 years. In addition, no siRNAs carrying viral sequences were found in the sea anemone *Actinia equina* (33), and failures of gene knockdown by dsRNA were reported in *Nematostella*(34), which points against the robust activity of antiviral RNAi pathway.

To address the contradicting evidence and answer the question if antiviral RNAi is an immune-related mechanism in cnidarians, here we characterize the antiviral RNAi response to dsRNA injection in *N. vectensis*.

Results

Injection of dsRNA results in mild and short-lived transgene knockdown

To test the activation of the antiviral RNAi pathway in *N. vectensis*, we utilized a transgenic line of anemones which expresses enhanced GFP (eGFP) ubiquitously under actin promoter (35). We injected dsRNA carrying the sequence of eGFP to heterozygous zygotes of this line and visualized the animals after 24 hours under a fluorescent stereomicroscope. As control, we injected dsRNA with a scrambled sequence of eGFP (srGFP). The fluorescence of eGFP is

dimmer in the embryos injected with eGFP dsRNA compared to srGFP (**Figure 1A**). We continued to track the fluorescence for 72 hours and documented that the difference in eGFP fluorescence between the injected groups is no longer visually distinguishable at this timepoint (**Figure 1B**). To validate this at the molecular level, we performed RT-qPCR and confirmed that at 24 hours eGFP transcripts are significantly lower in eGFP dsRNA injected animals; however, the level of knockdown is relatively modest, only 40 % compared to srGFP injected animals (**Figure 1C, supplementary file 1**). As expected, no significant difference in eGFP transcript level was detected by RT-qPCR at 72 hours after injection (**Figure 1D, supplementary file 1**).

Figure 1 – dsRNA injection to *N. vectensis* zygotes triggers mild gene knockdown

A. Heterozygous *actin::eGFP* embryos showing dimmer eGFP fluorescence 24 hours following injection of dsRNA carrying eGFP sequence (left) compared to injection of scrambled eGFP sequence (right). Scale bars represent 500 µm.
B. No difference in eGFP fluorescence of heterozygous *actin::eGFP* embryos is exhibited 72 hours following injection of dsRNA carrying eGFP sequence (left) compared to injection of scrambled eGFP sequence (right). Scale bars represent 500 µm.
C. eGFP transcript levels fold change measured by RT-qPCR, 24 hours following injection of dsRNA. Statistical significance is shown for pairwise comparison (one-tailed Student's t-test, n=3 biological replicates, p-value = 0.0268).
D. eGFP transcript levels fold change measured by RT-qPCR, 72 hours following injection of dsRNA. Statistical significance is shown for pairwise comparison (one-tailed Student's t-test, n=3 biological replicates, p-value = 0.4899).

dsRNA injection to *N. vectensis* zygotes leads to generation of siRNAs

The knockdown of eGFP following dsRNA injection suggested that the RNAi pathway was activated, hence, next we wished to investigate if siRNAs, which are the hallmark of antiviral RNAi in nematodes, flies and plants, were generated. To detect eGFP targeting siRNAs, we

generated small RNA libraries for both *actin::eGFP* heterozygotes and wild-type (WT) animals injected with eGFP dsRNA, at 24 hours post-injection. We mapped the 18-30 nucleotide (nt) long small RNA reads to eGFP sequence and revealed a significant enrichment of reads mapping to eGFP in groups injected with dsRNA compared to the mock injected controls (**Figure 2A, supplementary file 2**). Consistent with this, fluorescence intensity was weaker in dsRNA-injected *actin::eGFP* heterozygotes compared to controls (**Figure 2 supp**). As expected, there was no difference in read counts that map to eGFP between the *actin::eGFP* and the WT animals. Moreover, the size distribution of the reads showed that most of them are 20-21 nt long, which resembles to the length of siRNA in other organisms but one nucleotide shorter and is in accordance to endogenous siRNAs previously reported for *N. vectensis* (12,18,36) (**Figure 2B**). We then visualized the mapping locations to eGFP and interestingly found a reoccurring pattern between all replicates in both *actin::eGFP* and WT injected animals (**Figure 2C and D, supplementary file 3**). This indicates that reads mapping to eGFP are not a result of random degradation of the injected dsRNA but of mechanistic processing. The origin of the reads from the sense or antisense strand of the dsRNA also showed a recurring pattern between replicates (**Figure 2C and D, supplementary file 3**).

<u>Figure 2 – Primary siRNAs are generated following dsRNA injection</u>

A. Normalized number of reads mapping to eGFP sequence, from embryos injected with dsRNA carrying eGFP sequence. *Actin::eGFP* zygotes were injected with either dsRNA or mock injection mix. WT zygotes were injected with dsRNA. Statistical significance is shown for pairwise comparison (one-way ANOVA with Tukey's HSD post-hoc test, n=3 biological replicates, p-values = 0.0077625, 0.0306363, 0.4711136).

B. Size distribution of reads mapping to eGFP sequence corresponding to the samples in (A).

C-D. eGFP sequence coverage by small RNA reads from *actin::eGFP* (C) or WT (D) embryos injected with eGFP dsRNA. The top graph represents the sense strand, and the bottom graph represents the antisense strand. Biological replicates are represented by different colors.

No production of secondary siRNAs was detected

Secondary siRNAs production is a major part of antiviral RNAi response in *C. elegans* and *Drosophila*, which amplifies the response and inflicts stronger and longer silencing of viral RNA. Therefore, we wished to test if this process also occurs in *N. vectensis.* Since *N. vectensis* has four RdRPs, three of which are upregulated upon viral mimic injection (26), we hypothesized that secondary siRNAs might be produced by RdRPs, hence contain a 5' triphosphate moiety similarly to *C. elegans* secondary siRNAs (18). This modification prevents detection by 5'-ligation-dependent sequencing; thus, we applied treatment by RNA 5' Pyrophosphohydrolase (Rpph) to remove the modification and expose secondary siRNAs to ligation during small RNA libraries preparation. The treatment was applied to RNA extracted from *actin::eGFP* and WT embryos that were injected with eGFP dsRNA. The small RNA sequencing results revealed no significant difference in read counts mapping to eGFP between the Rpph-treated and untreated libraries (**Figure 3A, supplementary file 2**). In addition, there is no difference in the size distribution of the reads between the treatments, unlike similar experiments in *C. elegans* (**Figure 3B**) (18,19,21). These results concluded that no secondary siRNAs that chemically resemble the ones in *C. elegans* were generated. Nonetheless, unlike in nematodes and flies, most plants secondary siRNAs do not include 5' triphosphate, suggesting that absence of this modification cannot rule out by itself production of secondary siRNAs (16). Next, we took a different approach, based on a mechanism which occurs in *C. elegans*, in which secondary siRNAs are generated using the target mRNA as template for RNA dependent RNA replication (18,37). To test if this mechanism is active in *N. vectensis* we chose to inject into *actin::eGFP* transgenic zygotes a shorter eGFP dsRNA which includes only the 3' half of the original sequence and look for siRNAs that map upstream to it, covering the rest of the eGFP sequence. The presence of siRNAs mapping upstream of 3' half would suggest that the eGFP mRNA transcribed from the transgene is used as template for the transcription of the 5' siRNAs. Notably, following sequencing of small RNAs from half-eGFP compared to full-length-eGFP dsRNA injected animals, it was apparent that siRNA reads map

only to the 3' half of the eGFP (**Figure 3C, supplementary file 3**). The injection of half-eGFP was still able to knockdown eGFP levels, as eGFP transcript levels were not significantly different between half-eGFP and full-length-eGFP injected animals and fluorescence was similar (**Figure 3D and supp A, supplementary file 1)**. In addition, there was no difference between the number and size distribution of reads mapping to eGFP (**Figure 3 supp B and C, supplementary file 2**). Moreover, a recurring mapping pattern between replicates was observed, consistent with previous sequencing results (**Figure 3C, supplementary file 3**).

<u>Figure 3 – no secondary siRNAs were detected following dsRNA injection</u>

A. Normalized number of reads mapping to eGFP sequence following treatment of RNA with RppH enzyme or mock treatment. The treatment was performed on RNA extracted from *actin::eGFP* or WT embryos injected with dsRNA carrying eGFP sequence. Statistical significance is shown for pairwise comparison (one-way ANOVA with Tukey's HSD post-hoc test, n=3 biological replicates, p-values = 0.9940685, 0.9998878).
B. Size distribution of reads mapping to eGFP sequence corresponding to the samples in (A).
C. eGFP sequence coverage by small RNA reads from *actin::eGFP* embryos injected with 3' half-eGFP dsRNA. The top graph represents the sense strand, and the bottom graph represents the antisense strand. Biological replicates are represented by different colors.
D. eGFP transcript levels fold change measured by RT-qPCR, 24 hours following injection of either half-dsRNA or full length-dsRNA. Statistical significance is shown for pairwise comparison (one-tailed Student's t-test, n=3 biological replicates, p-value = 0.3848).

After learning that secondary siRNAs are not generated by similar mechanisms to *C. elegans*, we tested whether any species of siRNAs could be detected by removing a variety of RNA modifications, by performing panoramic RNA display by overcoming RNA modification aborted sequencing (PANDORA-seq) that combines treatments by T4 polynucleotide kinase and α-ketoglutarate-dependent hydroxylase and was shown to expose numerous types of modified small RNAs to sequencing (38). Mapping the reads from both PANDORA-seq and traditional small RNA sequencing to eGFP sequence did not reveal an increase in reads

mapping to eGFP or any major changes in mapping distribution (**Figure 4A, B, supplementary file 3**). The mapping peaks differ in read count which could be explained by the fact that PANDORA-seq detects a larger variety of small RNAs, hence decreasing the representation of dsRNA-originating siRNAs in the libraries. The size distribution of the reads mapping to eGFP also did not reveal a difference in siRNAs following the removal of modifications (**Figure 4C, D**).

<u>Figure 4 – Specific upregulation of antiviral RNAi components following dsRNA injection</u>

A-B. eGFP sequence coverage by small RNA reads sequenced by PANDORA-seq (A) or traditional small RNA sequencing (B). RNA was extracted from *actin::eGFP* embryos injected with dsRNA carrying eGFP sequence. The top graph represents the sense strand, and the bottom graph represents the antisense strand. The blue line represents the mean of n=4 biological replicates and the grey is the confidence interval.

C. Size distribution of reads mapping to eGFP sequence corresponding to the samples in (A).
D. Size distribution of reads mapping to eGFP sequence corresponding to the samples in (B).

E-H. Western blots of antiviral RNAi-related components AGO2 (E) and Dicer1 (F) and miRNA system specific components AGO1 (G) and GW182 (H) performed on protein content extracted from WT embryos, 48 hours following injection of poly(I:C) or NaCl control (protein sizes: AGO1 96 kDa, GW182 185 kDa, AGO2 122 kDa, and Dicer1 171 kDa).

I. Fold change of normalized band intensity corresponding to the Western blots in (E-H), showing RNAi-related components signal in response to poly(I:C) or NaCl control. Statistical significance is shown for pairwise comparison (two-tailed Student's t-test or Mann-Whitney-Wilcoxon Test, $n \geq 6$ biological replicates, p-values = 0.02551, 0.00193, 0.00001079, 0.004998 for AGO1, GW182, AGO2 and Dicer1 respectively).

<u>dsRNA injection leads to downregulation of miRNA system components</u>

N. vectensis is known to have a functional miRNA system which employs components such as Dicer1, AGO1 and AGO2 that were shown to be crucial for the early development of this species (29,39,40). It was shown that AGO1 specifically carries miRNAs and AGO2 carries both miRNAs and endogenous siRNAs (29). Another miRNA system component is GW182 (called TNRC6 in vertebrates) that has a homolog in *N. vectensis* and was shown to mediate gene silencing when expressed in heterologously mammalian cells (41). Previous results show that injection of poly(I:C), which mimics viral dsRNA, into *N. vectensis* zygotes leads to upregulation of AGO2 and Dicer1, but not AGO1 or GW182 on the RNA level (26). To further test the activation of the RNAi system in *N. vectensis* we performed Western blot using RNAi components specific antibodies following injection of poly(I:C) to zygotes. In accordance with previous results, the Western blot shows upregulation of AGO2 and Dicer1 (**Figure 4E, F**). Interestingly, AGO1 and GW182 that are miRNA specific components seem to be downregulated (**Figure 4G, H**). This was found to be statistically significant by comparison of normalized band intensities (**Figure 4I, supplementary file 4**). To assess the effect of the antiviral immune response on miRNAs expression levels, we analyzed miRNA expression after eGFP dsRNA injection. The total read count of all *N. vectensis* miRNAs was not affected (**Figure 4 supp A, supplementary file 5**). A total of 10-12 miRNAs were differentially expressed, with no clear trend regarding the function of their target genes (**Figure 4 supp B and C**).

Discussion

Antiviral RNAi is an ancestral pathway that provides crucial defense against viruses to nematodes and insects, both belonging to the superphylum Ecdysozoa. The contradicting evidence regarding its activity in cnidarians have motivated us to test whether it has a role in the sea anemone *Nematostella vectensis*. Using eGFP dsRNA injection to zygotes of *actin::eGFP* anemones, we show that antiviral RNAi response is activated and it results in a significant but mild silencing of eGFP expression. This comes in contrast to the striking effect of silencing by RNAi exhibited in other organisms (42,43). Nonetheless, we show that

siRNAs are generated by processing of dsRNA into 20-21 nt long small RNAs, in a sequence specific manner which repeats in all replicates. The highly reproducible pattern of the mapping suggests that Dicer has a sequence preference for processing of the injected dsRNA, as seen in previous experiments in mammalian cells (8). In addition, the recurrence of sense- or antisense-specific mapping of each small RNA resembles the preference of AGO to select one of the strands of the small RNA duplex it loads. This phenomenon is known from the miRNA pathway where the guide strand gets selected by AGO whereas the star (also called passenger strand) is ejected and eventually degraded, resulting in much higher representation of the guide strand in sequencing data (44,45). It was previously shown that injection of similar length dsRNA triggers upregulation of immune-related genes including of AGO2 and Dicer1 in *N. vectensis* (26). This suggests that the injection of eGFP dsRNA activated the antiviral RNAi response that resulted in the generation of siRNAs and knockdown of eGFP.

The short-lived and mild knockdown effect caused by dsRNA injection could be explained by the lack of secondary siRNA generation. Three different methods were used in this study to detect secondary siRNAs and resulted in no detection. Hypothetically there could be secondary siRNAs in *N. vectensis* carrying yet unidentified modification masking them from sequencing; however, the short-term knockdown effect strongly supports the notion that there is no secondary amplification of the RNAi response. This result correlates with the moderate knockdown effect and suggests that the siRNA-mediated antiviral response in *N. vectensis* is not amplified by secondary siRNA generation, unlike in nematodes, flies and plants. It can also explain the lack of siRNAs carrying viral sequences from natural sea anemone populations (33). Another factor that might contribute to the moderate effect is that apoptosis is activated in *N. vectensis* upon poly(I:C) injection to zygotes (46). Apoptosis is a mechanism of host defense against viruses and its increased activity at 24 hours post-injection could mean that a stronger RNAi response is not feasible or crucial in *N. vectensis*. It was shown that in mammalian cells the RNAi response is inhibited in cells that carry out the interferon response, and inhibition of the interferon pathway reveals a functional RNAi response in differentiated

mammalian cells (47,48). In *N. vectensis*, homologs of canonical vertebrate antiviral factors that take part in the interferon response are upregulated in response to poly(I:C) (26). Unlike in mammals where interferon and RNAi were shown to be mostly antagonistic one towards the other (49,50), knockdown of the dsRNA receptor RLRb, a homolog of the mammalian MDA5, in *N. vectensis* in combination with poly(I:C) injection leads to downregulation of AGO2 and Dicer1 (26), which hints that the interferon-like and RNAi pathways act in a synergetic manner in this species.

RNAi, especially in its form as homogenously-processed miRNAs, is an extremely useful tool to regulate gene expression levels, which could explain its wide conservation, even in organisms where alternative antiviral pathways have evolved (8,9). miRNAs tend to provide milder and more accurate regulation of expression levels compared to siRNAs and hence are less suitable for antiviral roles (51). Strikingly, the *N. vectensis* components that are specific to the miRNA pathway (AGO1 and GW182) are downregulated at the protein level under dsRNA challenge, whereas those that serve both miRNAs and siRNAs (Dicer1 and AGO2) are strongly upregulated (**Figure 4I**). A few cases of loss of the RNAi system have been described in fungi, but these are considered to have occurred recently in response to viral mechanisms that adapted to hijack the RNAi system and could have harmful effects in the long run (52,53). To fully understand the conservation of the antiviral RNAi system it must be characterized in other organisms from different phylogenetic lineages (54). Based on previous findings and the current study in *N. vectensis*, it could be concluded that RNAi as an antiviral response might be conserved as a helpful immune mechanism, even if it is not the main one. Furthermore, our work suggests that the synthesis of secondary siRNAs and the resulting long-term silencing of specific viruses by RNAi, might have been lost in sea anemones, as it is found in insects, nematodes and plants. Altogether this work challenges the common view that antiviral RNAi is the main immune mechanism of invertebrates in general and calls for further research of this system in other lineages.

Methods

Sea anemone culture and spawning

N. vectensis polyps were grown in the dark at 18 °C in 16 ‰ artificial sea water and fed three times a week with freshly hatched *Artemia salina* nauplii. Spawning and fertilization were conducted as previously described (40,55). *Actin::eGFP* anemones were kindly received from Dr. Aissam Ikmi (European Molecular Biology Laboratory, Heidelberg, Germany) (35). For injection to *actin::eGFP* line, sperm from heterozygous *actin::eGFP* males was used to fertilize WT eggs.

Microinjection of dsRNA

Microinjection to zygotes was performed with Eclipse Ti-S Inverted Research Microscopes (Nikon, Japan) connected to an Intensilight fiber fluorescent illumination system (Nikon) for visualization of the fluorescent injected mixture. The system is mounted with a NT88-V3 Micromanipulator Systems (Narishige, Japan). dsRNA carrying eGFP sequence was ordered from RiboPro (Netherlands) and SYNBIO technologies (USA) and was aliquoted and kept in -80 °C until use. All injection mixes included dextran Alexa Fluor 594 (Thermo Fisher Scientific, USA) as fluorescent tracer. dsRNA injected concentration was chosen according to survival of the injected animals, which was very low (i.e., below 50 %) above 7 ng/µl. For small RNA libraries eGFP dsRNA (RiboPro) was injected in concentration of 1.75 or 3.5 ng/µl (biological replicates of the same experiment were injected with the same concentration), to zygotes of *actin::eGFP* line or WT. The mock injection control included only water and tracer. Half-eGFP dsRNA was injected at the same molarity as full-length dsRNA. For RT-qPCR, eGFP dsRNA and srGFP (SYNBIO technologies) were injected at 7 ng/µl. For western blot, high molecular weight poly(I:C) (average size of 1.5–8 kb) in 0.9% NaCl (Invivogen, USA) was injected to WT zygotes in concentration of 6.25 ng/µl with 0.9% NaCl as control. Injected animals were kept in an incubator at 22 °C, counted and transferred to fresh 16 ‰ artificial sea water every day. The animals were visualized before being flash-frozen in liquid nitrogen and were kept in -80 °C until RNA extraction. All sequences used in this study appear in supplementary file 6.

RNA extraction

For generating small RNA libraries, total RNA was extracted from a few hundred injected animals using Tri-Reagent® (Merck Millipore, USA) according to the manufacturer's protocol, with minor changes. 1 µl of RNA-grade glycogen (Roche, Switzerland) was added into the isopropanol during the isolation step and centrifugation for isolation and 75% ethanol wash was at 21,130 × *g*. Final RNA pellets were re-suspended in 15-20 µl of RNase-free water (Biological Industries, Israel). RNA concentration was measured by Qubit™ RNA BR Assay Kit (Thermo Fisher Scientific). At this stage most of the extracted RNA was kept in -80 °C until small RNA libraries preparation and 400 ng were separated to use for RT-qPCR. The separated RNA was treated with Turbo DNase twice for 30 minutes at 37 °C (Thermo Fisher Scientific) to remove residual genomic DNA followed by another round of purification. RNA integrity was assessed by gel electrophoresis with 1:1 formamide (Merck Millipore) and 1 µl of loading dye on 1.5 % agarose gel for RT-qPCR and by Bioanalyzer Nanochip (Agilent, USA) for small RNA libraries. RNA that was not used for libraries was extracted using Quick-RNA microprep kit (Zymo Research, USA) with two rounds including Turbo DNase treatment.

Reverse transcription-quantitative PCR (RT-qPCR)

eGFP transcripts were amplified by RT-qPCR using primers designed via Primer3 version 0.4.0 (56), Primer calibration showed product specificity and 115 % efficiency, -2.99 slope and R2 >0.98. cDNA was prepared using iScript according to manufacturer's protocol (Bio-Rad, USA) and was diluted to 5 ng/µl and stored at -20 °C. RT-qPCR was performed using StepOnePlus Real-Time PCR System v2.2 (ABI, Thermo Fisher Scientific) with Fast SYBR Green Master Mix (Thermo Fisher Scientific). Each sample was quantified in triplicates for GFP transcript and housekeeping gene 4 (HKG4) as an internal control (57). 1 µl of cDNA template was used for each technical replicate. The Reaction thermal profile was 95 °C for 20 sec, then 40 amplification cycles of 95 °C for 3 sec and 60 °C for 30 sec, a dissociation cycle of 95 °C for 15 sec and 60 °C for 1 min and then brought back to 95 °C for 15 sec (+0.6 °C

steps). eGFP fold-change was analyzed using a comparative Ct method ($2^{-\Delta\Delta Ct}$) (58). All RT-qPCR experiments included three biological replicates. Primer sequences used in this study appear in supplementary file 6.

Small RNA library preparation

Between 0.5-1 µg of extracted RNA was mixed with spikeins (0.025 fmol per 1 µg of RNA) and size selected on 15% urea-PAGE gel (Bio-Rad). RNA in the size of 18-30 nucleotides was cut and extracted from gel by incubation overnight in 810 µl 0.3 M NaCl at 4 °C in rotation. Size-selected small RNAs were precipitated at -20 °C for a minimum of 3 hours in 1 ml ice-cold 100% ethanol with 1 µl glycogen (Merck Millipore), then washed with 900 µl of ice-cold 75% ethanol, centrifuged at 21,130 × *g* and resuspended in 7.5 µl RNase-free water. Next, small RNA libraries were prepared using NEBNext Multiplex Small RNA Library Prep Set for Illumina kit (New England Biolabs, USA) with some modifications (59). Library preparation kit adapters 3' and 5' and reverse transcription primer were diluted 1:1 of stock concentration before use. For overnight ligation of 3' adapter, T4 RNA Ligase 2 truncated KQ and Murine RNase inhibitor were used (New England Biolabs). The ligated products were subjected to 13-18 cycles of PCR amplification then Certified Low Range Ultra Agarose (Bio-Rad) stained with orange gel loading dye (New England Biolabs). Bands ranging between 137 and 149 nucleotides (corresponding to adapter ligated small RNAs) were cut from gel and purified using NucleoSpin Gel and PCR Clean-up (Macherey-Nagel, Germany) with elution volume of 12 µl. Final concentrations were measured using Qubit HS dsDNA assay kit (Thermo Fisher Scientific). The quality of cDNA libraries was checked by using TapeStation system on High Sensitivity D1000 ScreenTape (Agilent). The libraries were validated for a dominant peak at the size range of 150-167 nucleotides and sequenced with NextSeq500 (Illumina) in single end mode. Small RNA reads were analyzed using miRDeep2 (60). Sequences shorter than 18 nucleotides were not included. Filtered reads were mapped to *N. vectensis* genome using Bowtie1 (version 1.3.1) (61). Reads not mapped to the genome were then mapped to eGFP sequence. miRDeep2 quantifier.pl module was used with default

parameters for quantification of miRNA reads. Read counts were normalized to spikeins and multiplied by 10000 for read count comparison. The normalized reads were averaged between three biological replicates.

RNA 5' Pyrophosphohydrolase (RppH) treatment

To remove potential 5'-triphosphate modification from small RNAs, total RNA was divided to two reactions, one was treated with RppH enzyme (New England Biolabs) according to manufacturer's protocol and the control libraries were treated with no enzyme.

PANDORA-seq

PANDORA-seq was performed as described before (38). Briefly, total extracted RNAs were separated through a 15 % urea polyacrylamide gel and small RNAs of 15–50 nt were visualized with SYBR Gold solution (Invitrogen, USA). 15-50 nt small RNAs were excised and recovered by gel elution buffer as previously described (62). A sample of the eluted RNA was stored in -80 °C for traditional-seq, the remaining eluted RNA was then treated with T4 polynucleotide kinase (T4PNK) enzyme in a 50 µl reaction mixture (5 µl 10× PNK buffer, 1 mM ATP, 10 U T4PNK) followed by RNA isolation with TRIzol (Thermo Fisher Scientific). The collected RNAs were then treated with Alkane monooxygenase (AlkB) in a 50 µl reaction mixture (50 mM HEPES, 75 µM ferrous ammonium sulfate, 1 mM α-ketoglutaric acid, 2 mM sodium ascorbate, 50 mg/L BSA, 4 µg/mL AlkB, 2,000 U/mL RNase inhibitor) followed by RNA isolation with TRIzol. The small RNA libraries were prepared by NEBNext® Small RNA Library Prep Kit (New England Biolabs) as the manufacturer described. In short, the adapters were ligated sequentially (3′ adapter, reverse transcription primer, 5′ adapter). First-strand cDNA synthesis was performed followed by PCR amplification with PCR index primer and PCR Master Mix to enrich the cDNA fragments. Finally, the PCR products were purified from PAGE gel and prepared for sequencing. Small RNAs were sequenced using NovaSeq 6000 (Illumina) in paired-end mode. Reads were analyzed as described above (Small RNA library preparation), from one set of the paired

reads (R1) due to their short length. Read counts were normalized to reads unmapped to genome and multiplied by 1 million.

Western blot

Animals were mechanically homogenized in the following lysis buffer: 50 mM Tris-HCl (pH 7.4), 150 mM KCl, 0.5 % NP-40, 10 % glycerol, protease inhibitor cOmplete ULTRA tablets (Roche) and Protease Inhibitor Cocktail Set III, EDTA-Free (Merck Millipore), or alternatively HALT protease inhibitor (Thermo Fisher Scientific). Protease inhibitors were added fresh just before use. After 2 hours rotation in 4 °C the samples were centrifuged at 16,000 × *g* for 15 min at 4 °C and supernatant was collected. Protein concentration was measured using Pierce BCA Protein Assay Kit (Thermo Fisher Scientific). Equal amounts of protein were run on 4–15 % Mini-PROTEAN TGX Precast Protein Gel (Bio-Rad) followed by blotting to a polyvinylidene fluoride or nitrocellulose membrane (Bio-Rad). Next, the membrane was washed with TBST buffer (20 mM Tris pH 7.6, 150 mM NaCl, 0.1% Tween 20) and blocked with 5% skim milk (BD, USA) in TBST for 1 hour on the shaker at room temperature. Previously validated custom-made antibodies for *Nematostella* GW182 (41), Dicer1 (39), AGO1 and AGO2 (Genscript, USA) (29) or monoclonal mouse anti-GAPDH (Abcam, United Kingdom) serving as loading control were diluted 1:1,000 in TBST containing 5% BSA (MP Biomedicals, USA) and incubated with the membrane in a sealed sterile plastic bag at 4 °C overnight. The membrane was washed three times with TBST for 10 min and incubated for 1 h with 1:10,000 diluted peroxidase-conjugated anti-mouse, anti-rabbit or anti-Guinea pig antibody (Jackson ImmunoResearch, USA) in 5 % skim milk in TBST. Finally, the membrane was washed three times with TBST, and detection was performed with the Clarity ECL kit (Bio-Rad) according to the manufacturer's instructions and visualized with a CCD camera of the Odyssey Fc imaging system (Li-COR Biosciences, USA). Size determination was carried out by simultaneously running Precision Plus Protein Dual Color Protein Ladder (Bio-Rad) and scanning at 700 nm wavelength. Band intensities were measured using the ImageStudio software (Li-COR). Band intensities were normalized

according to the darkest band in each membrane then the normalized values of investigated proteins were divided by normalized values of GAPDH.

Microscopy

Fluorescence of eGFP protein was detected by SMZ18 stereomicroscope (Nikon) connected to an Intensilight fiber illumination fluorescent system (Nikon). Images were captured by DS-Qi2 SLR camera (Nikon) and were analyzed and processed with NIS-Elements Imaging Software (Nikon).

Statistical analysis

Statistical analysis of small RNA read counts was done with one-way ANOVA with Tukey's HSD post-hoc test. For read counts of half-eGFP and full length-eGFP one-tailed Student's t-test was used. Comparison of eGFP transcript levels was conducted with one-tailed Student's t-test, by comparing ΔCt values between groups. Comparison of Western blot band intensities was done with two-tailed Student's t-test or Mann-Whitney-Wilcoxon Test for non-normal data by comparing normalized band intensities of the poly(I:C) compared to NaCl injected samples. Normality of the data and homogeneity of variance was validated before every statistical analysis. All experiments included at least three biological replicates, and three technical replicates were added for RT-qPCR. The tests were performed in Rstudio 2021.09.0.

Data availability

All small RNA sequencing data in this paper are available on the SRA repository under identification number PRJNA1145188.

Reviewer link:
https://dataview.ncbi.nlm.nih.gov/object/PRJNA1145188?reviewer=36jpse10kih79r3t6akqk417nu

Acknowledgements

The authors thank Dr. Aissam Ikmi (European Molecular Biology Laboratory, Heidelberg, Germany) for the kind gift of *actin::eGFP* anemones and Dr. Michal Bronstein and Ms. Adi Turjeman (The Center for Genomic Technologies, The Hebrew University of Jerusalem, Israel) for their help with high-throughput sequencing.

Supporting information

Supplementary Figure 2 – eGFP knockdown in *actin::eGFP* embryos injected with dsRNA

A. Heterozygous *actin::eGFP* embryos showing dimmer eGFP fluorescence 24 hours following injection of dsRNA carrying eGFP sequence (left) compared to injection of mock injection mix (right). Scale bars represent 500 µm.
B. eGFP transcript levels fold change measured by RT-qPCR, 24 hours following injection of dsRNA. Statistical significance is shown for pairwise comparison (one-tailed Student's t-test, n=4 biological replicates, p-value = 0.02082).

Supplementary Figure 3 – eGFP knockdown in *actin::eGFP* embryos injected with dsRNA

A. Heterozygous *actin::eGFP* embryos showing dimmer eGFP fluorescence 24 hours following injection of 3' half- (left) or full length-dsRNA carrying eGFP sequence (middle) compared to injection of mock injection mix (right). Scale bars represent 500 µm.
B. Normalized number of reads mapping to eGFP sequence, from embryos injected with either 3' half- or full length-dsRNA carrying eGFP sequence, or mock injection mix. Statistical significance is shown for pairwise comparison (two-tailed Student's t-test, n=3 biological replicates, p-value = 0.8221).
C. Size distribution of reads mapping to eGFP sequence corresponding to the samples in (B).

Supplementary Figure 4 – miRNA levels are largely unaffected by dsRNA injection

A. Normalized total number of miRNAs reads from embryos injected with dsRNA. *Actin::eGFP* zygotes were injected with either dsRNA or mock injection mix. WT

zygotes were injected with dsRNA. Statistical significance is shown for pairwise comparison (one-way ANOVA with Tukey's HSD post-hoc test, n=3 biological replicates, p-values = 0.6853716, 0.9198027, 0.8905552).

B-C. Differentially expressed miRNAs in *actin::eGFP* (B) and WT (C) embryos following injection of dsRNA.

Supplementary file 1 - RT-qPCR data

Supplementary file 2 - small RNA sequencing read counts

Supplementary file 3 - eGFP coverage reads per base

Supplementary file 4 - Western blot band intensities

Supplementary file 5 - miRNAs read count

Supplementary file 6 - DNA sequences

References

1. Matranga C, Zamore PD. Small silencing RNAs. Current Biology. 2007 Sep 18;17(18):R789–93.

2. Wilson RC, Doudna JA. Molecular Mechanisms of RNA Interference. Annual Review of Biophysics. 2013 May 6;42(Volume 42, 2013):217–39.

3. Ding SW, Li H, Lu R, Li F, Li WX. RNA silencing: a conserved antiviral immunity of plants and animals. Virus Res. 2004 Jun 1;102(1):109–15.

4. Cerutti H, Casas-Mollano JA. On the origin and functions of RNA-mediated silencing: from protists to man. Curr Genet. 2006 Aug;50(2):81–99.

5. Nayak A, Tassetto M, Kunitomi M, Andino R. RNA interference-mediated intrinsic antiviral immunity in invertebrates. Curr Top Microbiol Immunol. 2013;371:183–200.

6. Stetson DB, Medzhitov R. Type I interferons in host defense. Immunity. 2006 Sep;25(3):373–81.

7. Ivashkiv LB, Donlin LT. Regulation of type I interferon responses. Nat Rev Immunol. 2014 Jan;14(1):36–49.

8. Flemr M, Malik R, Franke V, Nejepinska J, Sedlacek R, Vlahovicek K, et al. A Retrotransposon-Driven Dicer Isoform Directs Endogenous Small Interfering RNA Production in Mouse Oocytes. Cell. 2013 Nov 7;155(4):807–16.

9. Poirier EZ, Buck MD, Chakravarty P, Carvalho J, Frederico B, Cardoso A, et al. An isoform of Dicer protects mammalian stem cells against multiple RNA viruses. Science. 2021 Jul 9;373(6551):231–6.

10. Zamore PD, Tuschl T, Sharp PA, Bartel DP. RNAi: Double-Stranded RNA Directs the ATP-Dependent Cleavage of mRNA at 21 to 23 Nucleotide Intervals. Cell. 2000 Mar 31;101(1):25–33.

11. Bernstein E, Caudy AA, Hammond SM, Hannon GJ. Role for a bidentate ribonuclease in the initiation step of RNA interference. Nature. 2001 Jan;409(6818):363–6.

12. Elbashir SM, Lendeckel W, Tuschl T. RNA interference is mediated by 21- and 22-nucleotide RNAs. Genes Dev. 2001 Jan 15;15(2):188–200.

13. Hammond SM, Boettcher S, Caudy AA, Kobayashi R, Hannon GJ. Argonaute2, a Link Between Genetic and Biochemical Analyses of RNAi. Science. 2001 Aug 10;293(5532):1146–50.

14. Vaistij FE, Jones L, Baulcombe DC. Spreading of RNA Targeting and DNA Methylation in RNA Silencing Requires Transcription of the Target Gene and a Putative RNA-Dependent RNA Polymerase. The Plant Cell. 2002 Apr 1;14(4):857–67.

15. Garcia-Ruiz H, Takeda A, Chapman EJ, Sullivan CM, Fahlgren N, Brempelis KJ, et al. Arabidopsis RNA-Dependent RNA Polymerases and Dicer-Like Proteins in Antiviral Defense and Small Interfering RNA Biogenesis during Turnip Mosaic Virus Infection. The Plant Cell. 2010 Feb 1;22(2):481–96.

16. Willmann MR, Endres MW, Cook RT, Gregory BD. The Functions of RNA-Dependent RNA Polymerases in Arabidopsis. Arabidopsis Book. 2011 Jul 31;9:e0146.

17. Tassetto M, Kunitomi M, Andino R. Circulating Immune Cells Mediate a Systemic RNAi-Based Adaptive Antiviral Response in Drosophila. Cell. 2017 Apr 6;169(2):314-325.e13.

18. Pak J, Fire A. Distinct Populations of Primary and Secondary Effectors During RNAi in C. elegans. Science. 2007 Jan 12;315(5809):241–4.

19. Pak J, Maniar JM, Mello CC, Fire A. Protection from Feed-Forward Amplification in an Amplified RNAi Mechanism. Cell. 2012 Nov 9;151(4):885–99.

20. Félix MA, Ashe A, Piffaretti J, Wu G, Nuez I, Bélicard T, et al. Natural and Experimental Infection of Caenorhabditis Nematodes by Novel Viruses Related to Nodaviruses. PLOS Biology. 2011 Jan 25;9(1):e1000586.

21. Ashe A, Bélicard T, Le Pen J, Sarkies P, Frézal L, Lehrbach NJ, et al. A deletion polymorphism in the Caenorhabditis elegans RIG-I homolog disables viral RNA dicing and antiviral immunity. Weigel D, editor. eLife. 2013 Oct 8;2:e00994.

22. Poirier EZ, Goic B, Tomé-Poderti L, Frangeul L, Boussier J, Gausson V, et al. Dicer-2-Dependent Generation of Viral DNA from Defective Genomes of RNA Viruses Modulates Antiviral Immunity in Insects. Cell Host & Microbe. 2018 Mar;23(3):353-365.e8.

23. Technau U, Steele RE. Evolutionary crossroads in developmental biology: Cnidaria. Development. 2011 Apr;138(8):1447–58.

24. Layden MJ, Rentzsch F, Röttinger E. The rise of the starlet sea anemone Nematostella vectensis as a model system to investigate development and regeneration. WIREs Developmental Biology. 2016;5(4):408–28.

25. Kayal E, Bentlage B, Sabrina Pankey M, Ohdera AH, Medina M, Plachetzki DC, et al. Phylogenomics provides a robust topology of the major cnidarian lineages and insights on the origins of key organismal traits. BMC Evolutionary Biology. 2018 Apr 13;18(1):68.

26. Lewandowska M, Sharoni T, Admoni Y, Aharoni R, Moran Y. Functional Characterization of the Cnidarian Antiviral Immune Response Reveals Ancestral Complexity. Molecular Biology and Evolution. 2021 Oct 1;38(10):4546–61.

27. Margolis SR, Dietzen PA, Hayes BM, Wilson SC, Remick BC, Chou S, et al. The cyclic dinucleotide 2'3'-cGAMP induces a broad antibacterial and antiviral response in the sea anemone Nematostella vectensis. Proc Natl Acad Sci U S A. 2021 Dec 21;118(51):e2109022118.

28. Jiang X, Kinch LN, Brautigam CA, Chen X, Du F, Grishin NV, et al. Ubiquitin-Induced Oligomerization of the RNA Sensors RIG-I and MDA5 Activates Antiviral Innate Immune Response. Immunity. 2012 Jun 29;36(6):959–73.

29. Fridrich A, Modepalli V, Lewandowska M, Aharoni R, Moran Y. Unravelling the developmental and functional significance of an ancient Argonaute duplication. Nat Commun. 2020 Dec 3;11(1):6187.

30. Lohmann JU, Endl I, Bosch TCG. Silencing of Developmental Genes in *Hydra*. Developmental Biology. 1999 Oct 1;214(1):211–4.

31. Chera S, de Rosa R, Miljkovic-Licina M, Dobretz K, Ghila L, Kaloulis K, et al. Silencing of the hydra serine protease inhibitor Kazal1 gene mimics the human SPINK1 pancreatic phenotype. J Cell Sci. 2006 Mar 1;119(Pt 5):846–57.

32. Dunn SR, Phillips WS, Green DR, Weis VM. Knockdown of Actin and Caspase Gene Expression by RNA Interference in the Symbiotic Anemone Aiptasia pallida. The Biological Bulletin. 2007 Jun;212(3):250–8.

33. Waldron FM, Stone GN, Obbard DJ. Metagenomic sequencing suggests a diversity of RNA interference-like responses to viruses across multicellular eukaryotes. PLOS Genetics. 2018 Jul 30;14(7):e1007533.

34. Reitzel AM, Ryan JF, Tarrant AM. Establishing a model organism: a report from the first annual Nematostella meeting. Bioessays. 2012 Feb;34(2):158–61.

35. He S, Del Viso F, Chen CY, Ikmi A, Kroesen AE, Gibson MC. An axial Hox code controls tissue segmentation and body patterning in Nematostella vectensis. Science. 2018 Sep 28;361(6409):1377–80.

36. Moran Y, Fredman D, Praher D, Li XZ, Wee LM, Rentzsch F, et al. Cnidarian microRNAs frequently regulate targets by cleavage. Genome Res. 2014 Apr;24(4):651–63.

37. Sijen T, Fleenor J, Simmer F, Thijssen KL, Parrish S, Timmons L, et al. On the Role of RNA Amplification in dsRNA-Triggered Gene Silencing. Cell. 2001 Nov 16;107(4):465–76.

38. Shi J, Zhang Y, Tan D, Zhang X, Yan M, Zhang Y, et al. PANDORA-seq expands the repertoire of regulatory small RNAs by overcoming RNA modifications. Nat Cell Biol. 2021 Apr;23(4):424–36.

39. Modepalli V, Fridrich A, Agron M, Moran Y. The methyltransferase HEN1 is required in Nematostella vectensis for microRNA and piRNA stability as well as larval metamorphosis. PLOS Genetics. 2018 Aug 17;14(8):e1007590.

40. Tripathi AM, Admoni Y, Fridrich A, Lewandowska M, Surm JM, Aharoni R, et al. Functional characterization of a 'plant-like' HYL1 homolog in the cnidarian Nematostella vectensis indicates a conserved involvement in microRNA biogenesis. Ketting R, Weigel D, Ketting RF, editors. eLife. 2022 Mar 15;11:e69464.

41. Mauri M, Kirchner M, Aharoni R, Ciolli Mattioli C, van den Bruck D, Gutkovitch N, et al. Conservation of miRNA-mediated silencing mechanisms across 600 million years of animal evolution. Nucleic Acids Res. 2017 Jan 25;45(2):938–50.

42. Fire A, Xu S, Montgomery MK, Kostas SA, Driver SE, Mello CC. Potent and specific genetic interference by double-stranded RNA in Caenorhabditis elegans. Nature. 1998 Feb;391(6669):806–11.

43. Li H, Li WX, Ding SW. Induction and Suppression of RNA Silencing by an Animal Virus. Science. 2002 May 17;296(5571):1319–21.

44. Lim LP, Lau NC, Weinstein EG, Abdelhakim A, Yekta S, Rhoades MW, et al. The microRNAs of Caenorhabditis elegans. Genes Dev. 2003 Apr 15;17(8):991–1008.

45. Bartel DP. Metazoan MicroRNAs. Cell. 2018 Mar 22;173(1):20–51.

46. Kozlovski I, Jaimes-Becerra A, Sharoni T, Lewandowska M, Karmi O, Moran Y. Induction of apoptosis by double-stranded RNA was present in the last common ancestor of cnidarian and bilaterian animals. PLOS Pathogens. 2024 Jul 16;20(7):e1012320.

47. Maillard PV, Van der Veen AG, Deddouche□Grass S, Rogers NC, Merits A, Reis e Sousa C. Inactivation of the type I interferon pathway reveals long double□stranded RNA□mediated RNA interference in mammalian cells. The EMBO Journal. 2016 Dec;35(23):2505–18.

48. Seo GJ, Kincaid RP, Phanaksri T, Burke JM, Pare JM, Cox JE, et al. Reciprocal Inhibition between Intracellular Antiviral Signaling and the RNAi Machinery in Mammalian Cells. Cell Host & Microbe. 2013 Oct 16;14(4):435–45.

49. Witteveldt J, Ivens A, Macias S. Inhibition of Microprocessor Function during the Activation of the Type I Interferon Response. Cell Rep. 2018 Jun 12;23(11):3275–85.

50. Witteveldt J, Knol LI, Macias S. MicroRNA-deficient mouse embryonic stem cells acquire a functional interferon response. Elife. 2019 Apr 23;8:e44171.

51. Moran Y, Agron M, Praher D, Technau U. The evolutionary origin of plant and animal microRNAs. Nat Ecol Evol. 2017 Feb 21;1(3):27.

52. Nicolás FE, Garre V. RNA Interference in Fungi: Retention and Loss. Microbiol Spectr. 2016 Dec;4(6).

53. Drinnenberg IA, Fink GR, Bartel DP. Compatibility with killer explains the rise of RNAi-deficient fungi. Science. 2011 Sep 16;333(6049):1592.

54. Iwama RE, Moran Y. Origins and diversification of animal innate immune responses against viral infections. Nat Ecol Evol. 2023 Feb;7(2):182–93.

55. Genikhovich G, Technau U. Induction of spawning in the starlet sea anemone Nematostella vectensis, in vitro fertilization of gametes, and dejellying of zygotes. Cold Spring Harb Protoc. 2009 Sep;2009(9):pdb.prot5281.

56. Untergasser A, Cutcutache I, Koressaar T, Ye J, Faircloth BC, Remm M, et al. Primer3--new capabilities and interfaces. Nucleic Acids Res. 2012 Aug;40(15):e115.

57. Columbus-Shenkar YY, Sachkova MY, Macrander J, Fridrich A, Modepalli V, Reitzel AM, et al. Dynamics of venom composition across a complex life cycle. Sánchez Alvarado A, editor. eLife. 2018 Feb 9;7:e35014.

58. Schmittgen TD, Livak KJ. Analyzing real-time PCR data by the comparative CT method. Nat Protoc. 2008 Jun;3(6):1101–8.

59. Plotnikova A, Kellner MJ, Schon MA, Mosiolek M, Nodine MD. MicroRNA Dynamics and Functions During Arabidopsis Embryogenesis. The Plant Cell. 2019 Dec 1;31(12):2929–46.

60. Friedländer MR, Mackowiak SD, Li N, Chen W, Rajewsky N. miRDeep2 accurately identifies known and hundreds of novel microRNA genes in seven animal clades. Nucleic Acids Res. 2012 Jan;40(1):37–52.

61. Langmead B, Trapnell C, Pop M, Salzberg SL. Ultrafast and memory-efficient alignment of short DNA sequences to the human genome. Genome Biol. 2009;10(3):R25.

62. Nilsen TW. Gel purification of RNA. Cold Spring Harb Protoc. 2013 Feb 1;2013(2):180–3.

A

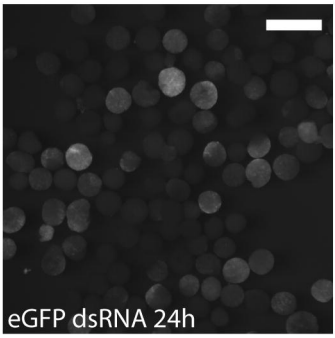
eGFP dsRNA 24h

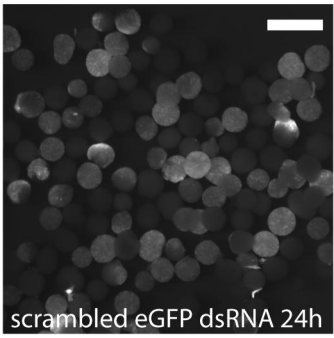
scrambled eGFP dsRNA 24h

B

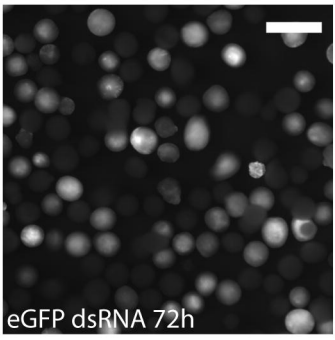
eGFP dsRNA 72h

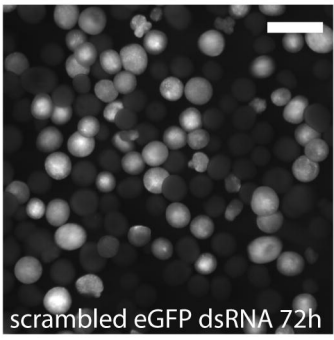
scrambled eGFP dsRNA 72h

C

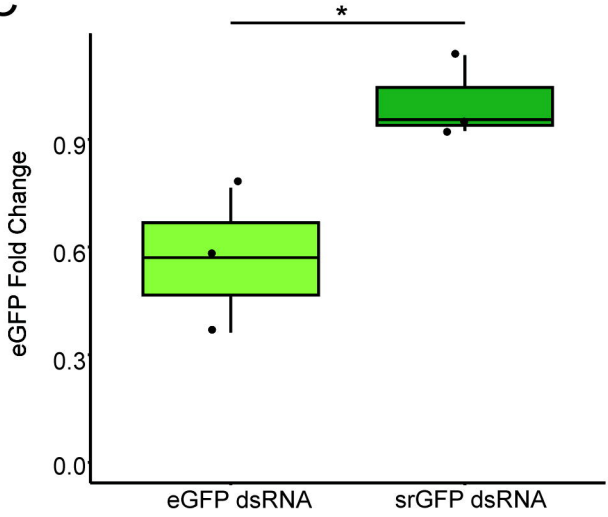
*
eGFP Fold Change
0.9
0.6
0.3
0.0
eGFP dsRNA
srGFP dsRNA

D

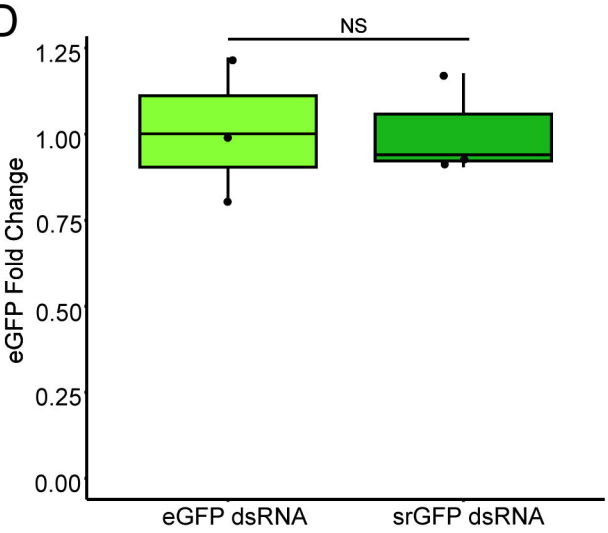
NS
eGFP Fold Change
1.25
1.00
0.75
0.50
0.25
0.00
eGFP dsRNA
srGFP dsRNA

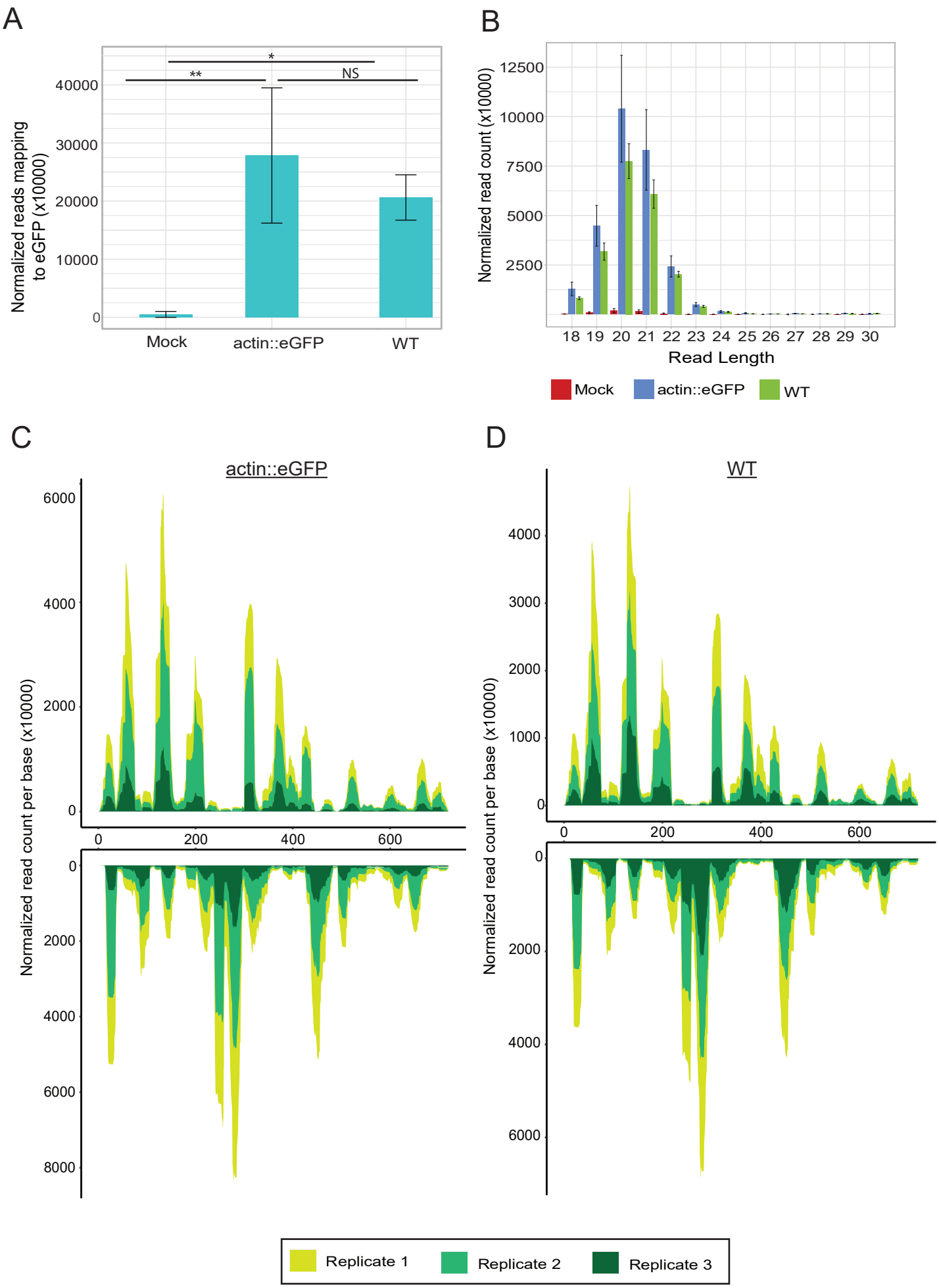
A
Normalized reads mapping to eGFP (x10000)
40000
30000
20000
10000
0
*
**
NS
Mock
actin::eGFP
WT
B
Normalized read count (x10000)
12500
10000
7500
5000
2500
18 19 20 21 22 23 24 25 26 27 28 29 30
Read Length
Mock
actin::eGFP
WT
C
actin::eGFP
Normalized read count per base (x10000)
6000
4000
2000
0
0
200
400
600
0
2000
4000
6000
8000
D
WT
Normalized read count per base (x10000)
4000
3000
2000
1000
0
0
200
400
600
0
2000
4000
6000
Replicate 1
Replicate 2
Replicate 3

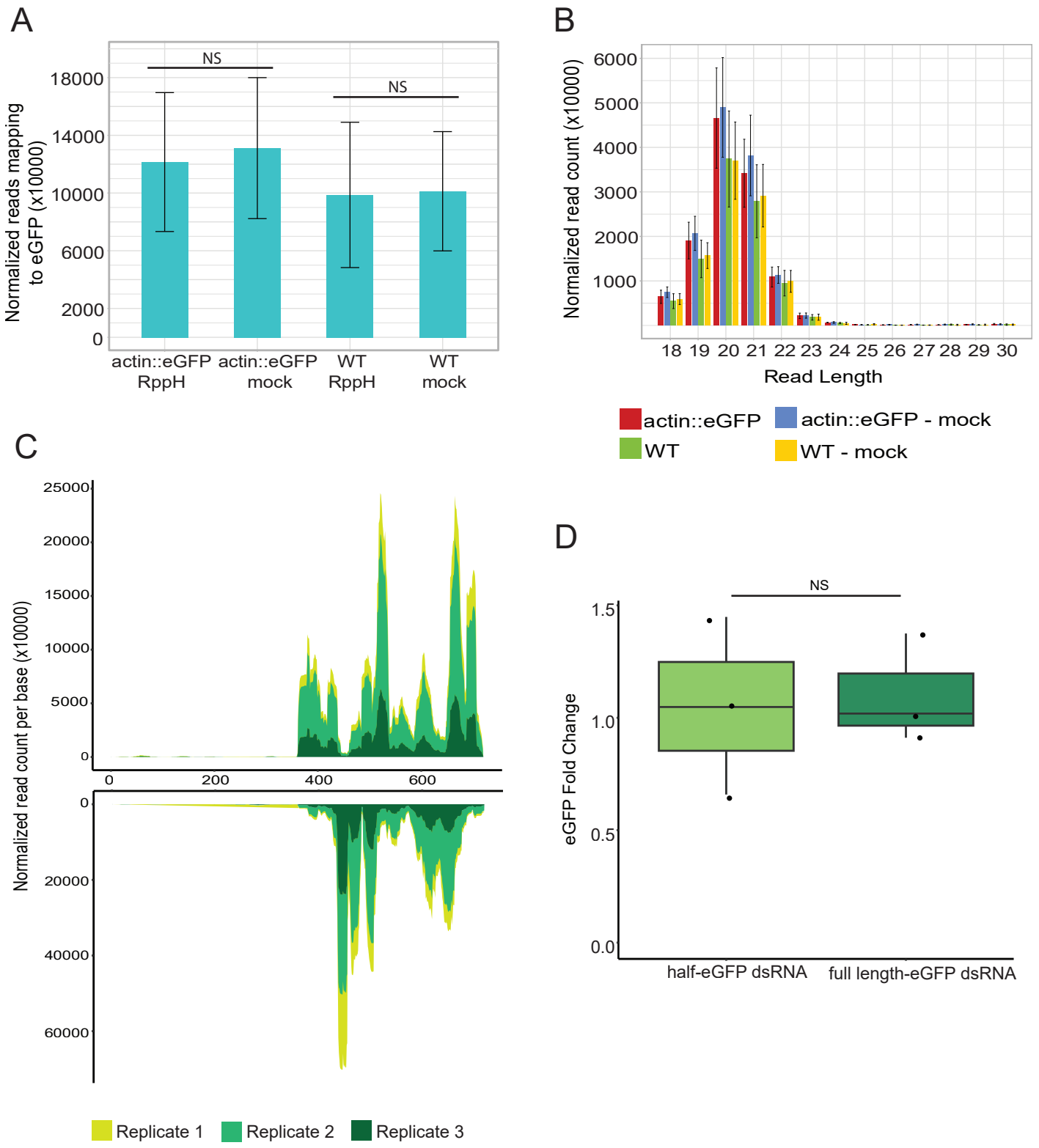
A
NS
NS
Normalized reads mapping to eGFP (x10000)
18000
14000
10000
6000
2000
0
actin::eGFP RppH
actin::eGFP mock
WT RppH
WT mock
B
Normalized read count (x10000)
6000
5000
4000
3000
2000
1000
18 19 20 21 22 23 24 25 26 27 28 29 30
Read Length
actin::eGFP
actin::eGFP - mock
WT
WT - mock
C
Normalized read count per base (x10000)
25000
20000
15000
10000
5000
0
0 200 400 600
0
20000
40000
60000
Replicate 1
Replicate 2
Replicate 3
D
NS
eGFP Fold Change
1.5
1.0
0.5
0.0
half-eGFP dsRNA
full length-eGFP dsRNA

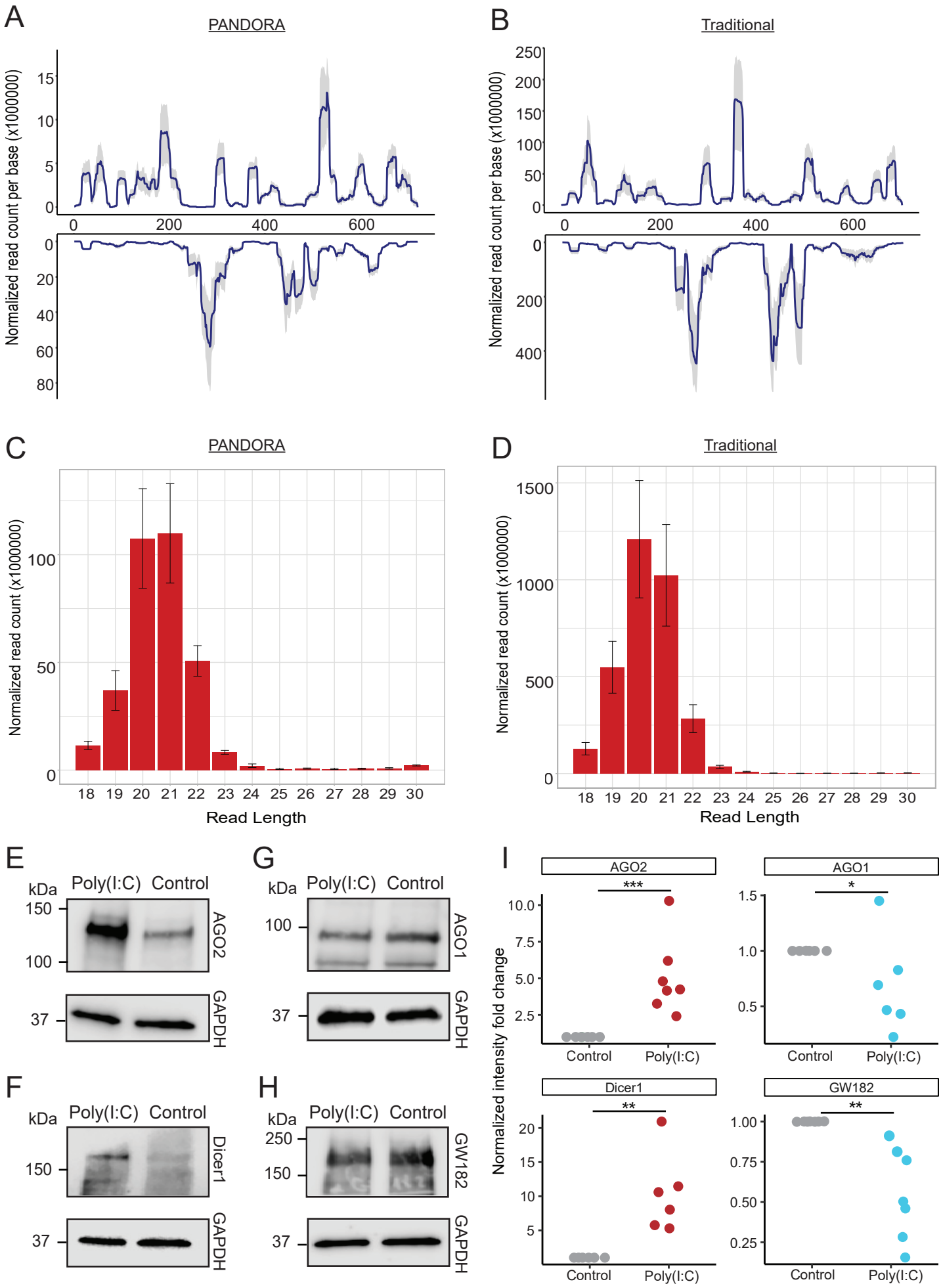
A
PANDORA
Normalized read count per base (x1000000)
B
Traditional
Normalized read count per base (x1000000)
C
PANDORA
Normalized read count (x1000000)
Read Length
D
Traditional
Normalized read count (x1000000)
Read Length
E
kDa
Poly(I:C)
Control
150
100
37
AGO2
GAPDH
G
kDa
Poly(I:C)
Control
100
37
AGO1
GAPDH
F
kDa
Poly(I:C)
Control
150
37
Dicer1
GAPDH
H
kDa
Poly(I:C)
Control
250
150
37
GW182
GAPDH
I
AGO2
AGO1
Dicer1
GW182
Normalized intensity fold change
Control
Poly(I:C)